Astronomy & Astrophysics manuscript no. output
June 18, 2020

SN 2018ijp: the explosion of a stripped-envelope star within a dense H-rich shell?

L. Tartaglia[1] and Friends

Department of Astronomy and the Oskar Klein Centre, Stockholm University, AlbaNova, SE 106 91 Stockholm, Sweden
(e-mail: leonardo.tartaglia@astro.su.se)

June 18, 2020

ABSTRACT

In this paper, we discuss the outcomes of the follow-up campaign of SN 2018ijp, discovered by the Zwicky Transient Facility survey for optical transients. SN 2018ijp shows early spectra similar to broad-lined supernovae of Type Ic around maximum light, followed later by strong signatures of interaction between rapidly expanding supernova ejecta and a dense H-rich circumstellar medium, coinciding with a second peak in the photometric evolution of the transient. Modeling the early luminosity of SN 2018jp results in $1.5\,M_\odot$ and $0.3\,M_\odot$ for the total ejected and radioactive ^{56}Ni masses, with an explosion energy of 6.5×10^{51} erg, while the analysis of the light curve at later phases suggests a total mass of $\simeq 0.5\,M_\odot$ for the H-rich circumstellar medium. Based on these results, obtained using simple analytical models, we discuss the observables of SN 2018jp in the context of the explosion of a massive star depleted of its outer H and He layers within a dense H-rich medium.

Key words. Supernovae: general – Supernovae: individual: SN 2018ijp

1. Introduction

A supernova (SN) is the most spectacular way a star can end its life, where progenitors more massive than $8-9\,M_\odot$ (see, e.g., Heger et al. 2003; Smartt 2009) are expected to explode as core-collapse (CC) SNe.

SNe interacting with a dense circumstellar medium (CSM) can produce a wide range of observables, resulting in a large heterogeneity of photometric and/or spectroscopic features. The classification of interacting transients is typically based on the presence of narrow emission features in their spectra, with Type IIn (Schlegel 1990) or Ibn (Pastorello et al. 2016; Hosseinzadeh et al. 2019) SNe being those showing prominent narrow H or He lines, respectively.

The current picture for the most common narrow-lined interacting SNe is that of fast moving ejecta colliding with a slow-moving dense CSM. In the shocked regions, a characteristic “forward-reverse" shock structure forms, and energetic UV photons can ionize the surrounding medium producing the structured, multi-component profiles occasionally observed in SNe IIn (see, e.g., Taddia et al. 2020). In this context, narrow lines (full–width–at–half–maximum – FWHM – of a few $10^2\,\mathrm{km\,s^{-1}}$) are recombination features produced in the slow-moving, unshocked CSM.

This requires the presence of a dense CSM produced by the progenitor star prior to its explosion, and seems to suggest massive luminous blue variables (LBVs), red supergiants (RSG) with super-winds (see, e.g., Smith et al. 2009; Yoon & Cantiello 2010) or Wolf-Rayet (WR) stars in binary systems as candidate progenitors for SNe IIn and Ibn. Such stars are all able to produce the dense and massive environment required to produce strong signatures of interaction, in some cases continuing years after the SN explosion (see, e.g., Tartaglia et al. 2020).

On the other hand, strong ejecta-CSM interaction can occur in any kind of explosion or stellar outburst and hence prevent the observer to collect information about the nature of the transient, including the explosion mechanism triggering the SN explosion. This is the case of the sub-class of interacting transients known as SNe Ia-CSM (see, e.g., Silverman et al. 2013), which are believed to be thermonuclear explosions embedded in a dense H-rich medium. While the nature of a few objects has been a matter of discussion (see, e.g., the different interpretations to explain SN 2002ic; Hamuy et al. 2003; Benetti et al. 2006) some observational signatures (e.g., a lack of strong Hβ and He I emission features) seem to be recurrent in these transients (Silverman et al. 2013).

Signatures of strong interaction, occasionally delayed with respect to the SN explosion, have been observed also in stripped-envelope (SE) SNe, optical transients typically showing a lack of H (SNe IIb and Ib) or both H and He features in their optical spectra (SNe Ic; see, e.g., Modjaz et al. 2014). A few recent examples of SNe showing a similar evolution are SNe 2014C (Milisavljevic et al. 2015; Margutti et al. 2017), 2017dio (Kuncarayakti et al. 2018) and 2017ens (Chen et al. 2018), all interpreted as CC SN explosions of SE SNe Ic within a dense, H-rich medium, with a possible progenitor scenario being that of a massive CSM produced during the RSG stage or by a stellar companion (e.g., Milisavljevic et al. 2015).

In this context, we present the results of our follow-up campaign of SN 2018ijp, discovered by the Zwicky Transient Facility (ZTF; Graham et al. 2019; Bellm et al. 2019) during the first year of operations. The transient was discovered in the host SDSS J102137.72+085554.1 on 2018 November 7.41 UT and labelled ZTF18aceqrrs[1]. The photometric and spectroscopic follow-up campaigns were triggered soon after discovery and a description of the facilities used and the reduction steps performed to obtained final light curves and spectra are described in Sect. 2. SN 2018ijp showed a relatively fast photometric evo-

[1] https://lasair.roe.ac.uk/object/ZTF18aceqrrs/

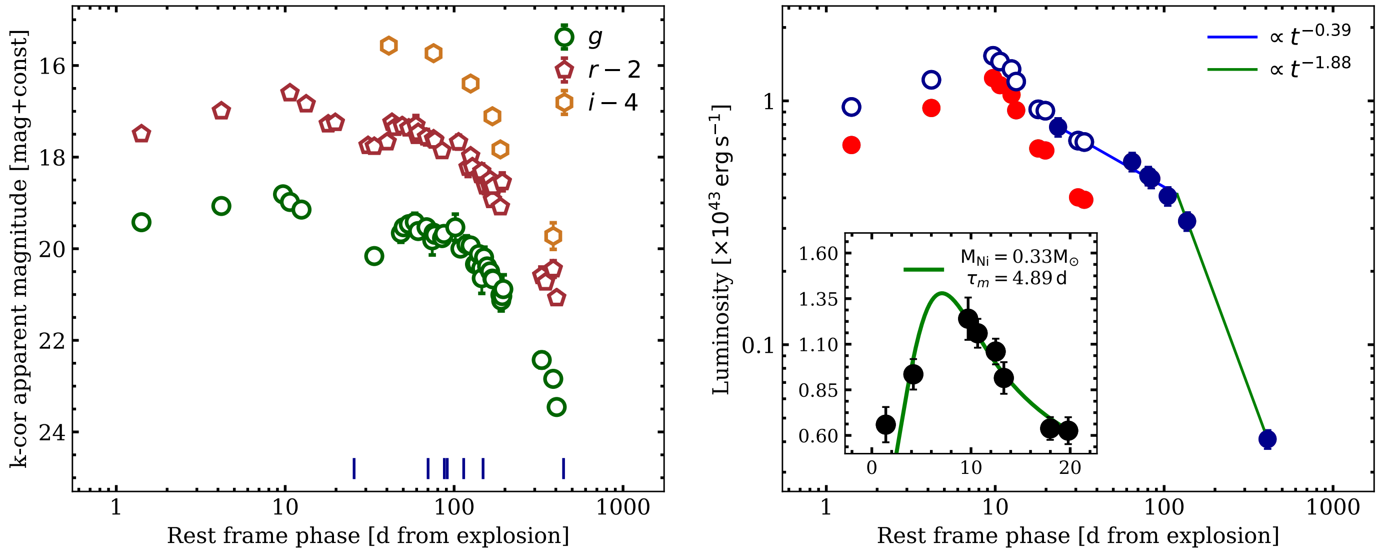

Fig. 1. Left: The *gri* light curves of SN 2018ijp, k-corrected and in rest frame. Blue ticks at the bottom mark the epochs of spectroscopic observations. **Right:** Bolometric light curve of SN 2018ijp estimated following the prescriptions of Lyman et al. (2014) (red points) and by fitting the SEDs obtained from the spectra (solid blue points). An estimate of the early peak obtained matching the luminosities obtained between ≃ +31 and +34 d is also shown (open blue points). The inset shows the fit of the model of Arnett (1982) to the early luminosity evolution of SN 2018ijp, resulting in $M_{Ni} \simeq 0.3\,M_\odot$ and $\tau_m \simeq 4.89 \pm 0.80$ d, corresponding to $E_k = (6.53 \pm 0.35) \times 10^{51}$ erg and $M_{ej} \simeq 1.6\,M_\odot$.

lution with double-peaked $g-$ and $r-$band light curves, with spectra showing strong signatures of delayed interaction with a dense pre-existing H-rich CSM in the form of narrow H lines in emission increasing their strength with time and a spectral continuum becoming significantly bluer with time, as described in Sect. 3. While interaction features dominate the evolution of SN 2018ijp at later times, we note that the spectrum around the first peak resembles those typical of a subclass of broad-lined Type Ic SNe (Ic-BL SNe; see, e.g., Taddia et al. 2019, and references therein), with a good match to the Type Ic-BL SN 1997ef (Mazzali et al. 2000). In addition, modeling the first peak in the context of a radioactively powered light curve gives ^{56}Ni and total ejected masses comparable with those obtained for the Type Ic-BL SN iPTF15dqg (Taddia et al. 2019). In Sect. 3.5, and throughout the rest of this paper, we will therefore discuss the observables of SN 2018ijp in the context of a massive, SE star within a dense H-rich medium.

In the following, we adopt a foreground Galactic extinction $E(B-V) = 0.029$ mag along the line of sight of SN 2018ijp, as estimated by Schlafly & Finkbeiner (2011) using a standard extinction law with $R_V = 3.1$ (Cardelli et al. 1989). We did not include any additional contribution from the local environment to the total extinction, since we could not identify strong Na ID features at the redshift of the host in the spectra of SN 2018ijp (see Sect. 3.2). The distance to SN 2018ijp was computed from the redshift derived using host lines (see Sect. 3.2) assuming a standard cosmology with $H_0 = 73\,\mathrm{km\,s^{-1}\,Mpc^{-1}}$, $\Omega_M = 0.27$ and $\Omega_\Lambda = 0.73$, resulting in a luminosity distance $D_L = 373$ Mpc[2].

2. Observations and data reduction

Th follow-up campaign of SN 2018ijp started on 2018, November 7.5 UT with the first detection of the transient. Photometry of the transient was mostly obtained using the Samuel Oschin telescope with the ZTF camera (P48; Dekany et al. 2020) in *g* and *r* bands. Additional photometry was obtained with the Nordic Optical Telescope (NOT) using the Alhambra Faint Object Spectrograph and Camera (ALFOSC[3]) and the Liverpool Telescope (LT) with the optical imaging component of the IO (Infrared-Optical) suite of instruments (IO:O[4]). P48 frames were obtained through the NASA/IPAC Infrared Science Archive[5], while magnitudes for these data were obtained using the dedicated pipeline SNOoPY[6]. The *i*−band photometry was obtained with the Palomar 60-inch telescope (P60) with SED Machine (SEDM) and reduced using the FPipe pipeline (Fremling et al. 2016). A log of the spectroscopic observations is reported in Table 1, including the names of the instruments used and basic information about the spectra. The classification spectrum, along with three additional spectra, were obtained with the Keck-I telescope using the Low Resolution Imaging Spectrograph (LRIS; Oke et al. 1994) and reduced using the automated pipeline LPipe (Perley 2019). Three additional spectroscopic observations were performed using the NOT with ALFOSC, reduced using foscgui[7]. An additional intermediate resolution spectrum was obtained using the ESO Very Large Telescope (VLT) with the X-shooter echelle spectrograph (Vernet et al. 2011), reduced using the ESO dedicated pipeline through the esoreflex environment (Freudling et al. 2013).

3. Analysis and discussion

3.1. Photometry

Pre-SN observations of the field of SN 2018ijp were obtained by ZTF since 2018 March 31.3 UT, resulting in no detections down

[2] Derived using CosmoCalc (Wright 2006) available at: http://www.astro.ucla.edu/~wright/CosmoCalc.html

[3] http://www.not.iac.es/instruments/alfosc/
[4] https://telescope.livjm.ac.uk/TelInst/Inst/IOO/
[5] https://irsa.ipac.caltech.edu/Missions/ztf.html
[6] http://graspa.oapd.inaf.it/snoopy.html
[7] http://graspa.oapd.inaf.it/foscgui.html

to average magnitudes of $\simeq$ 21mag in both g and r bands. Last non-detection limits were obtained on 2018 November 4.5 UT (corresponding to $g > 20.6$ and $r > 21.4$ mag), roughly three days before the first $g-$ and $r-$band detections. We will therefore adopt 2018 November 6.0 UT (JD = 2458428.5) as an estimate of the explosion epoch of SN 2018ijp and refer to phases with respect to this date. Magnitudes at rest frame epochs were obtained computing k-corrections using the spectra of SN 2018ijp and following the prescriptions of Hogg et al. (2002, see their Eq. 13), adopting a recessional velocity of $cz = 25540\,\mathrm{km\,s^{-1}}$, as derived from the redshift estimated from the host lines in the X-shooter spectrum ($z = 0.0852$; see Sect. 3.2). The resulting gri light curves are shown in Fig. 1 (left panel), along with an estimate of the bolometric luminosity of SN 2018ijp (right panel), which will be discussed below.

The early photometric evolution is fast, with both $g-$ and $r-$band light curves rapidly rising to a first maximum within $\simeq 8$ d from the SN explosion. At $\simeq +34$ d both the $g-$ and $r-$band light curves show a further rise to a second and broader peak (lasting $\simeq 25$ d), while the $i-$band light curve does not reveal the same 'double-peaked' shape due to lack of early observations in this band. After the second peak, the photometric evolution is slower in all bands, with decline rates of $\simeq 0.012$, 0.011 and $0.013\,\mathrm{mag\,d^{-1}}$ in $g-$, $r-$ and $i-$band, respectively. Rise times in g and r were computed fitting the early evolution in each band with a second-order polynomial in order to estimate the epoch of the maximum in each band. We note, in addition, that the photometric evolution during the rise is well reproduced by power-laws of the form $L_g \propto t^{0.29}$ and $L_r \propto t^{0.41}\,\mathrm{erg\,s^{-1}}$, with fluxes in g and r computed using the zero-points for the ZTF filters reported in the Spanish Virtual Observatory (SVO[8]; Rodrigo et al. 2012) after correcting the magnitudes for the Galactic extinction. Rise times were estimated simply assuming $t_{max} - t_{expl}$, corresponding to $t_{rise,g} = 7.9 \pm 1.5$ and $t_{rise,r} = 10.7 \pm 1.5$ d, where the errors are dominated by the uncertainty on the explosion epoch. These rise times are slightly smaller than the average $r-$band rise time inferred by Taddia et al. (2015) and Taddia et al. (2019) for their samples of SNe Ic-BL ($\simeq 14.7$ and $\simeq 15$ d, respectively), although still comparable with the low-end of the Ic-BL iPTF distribution presented in Taddia et al. (2019).

The $g - r$ early (i.e., at $t \lesssim 10$ d) color evolution is relatively fast, with the color index increasing from $\simeq 0.15$ to $\simeq 0.60$ mag. At later times, the $g - r$ index evolves toward bluer colors until $\simeq +80$ d, remaining roughly constant ($\simeq 0.1$ mag) throughout the rest of the photometric evolution of SN 2018ijp. At $t \gtrsim +60$ d, we note an almost linear decline in $r-i$, with the color index becoming progressively bluer with time, as reflected by the evolution of the pseudo-continuum observed in the spectra of SN 2018ijp (see Sect. 3.2).

Absolute magnitudes were obtained, after correcting apparent values for the Galactic reddening and adopting a distance modulus $\mu = 37.85$ mag (see Sect. 1). The resulting $M_{r,peak}$ falls within the upper end of the distribution of peak magnitudes presented in Taddia et al. (2019).

3.1.1. Evolution of the bolometric luminosity

An estimate of the early ($t \lesssim +20$ d) bolometric light curve of SN 2018ijp was obtained following the prescriptions of Lyman et al. (2014, see their Eq. 6 for their sample of SE SNe), allowing an estimate of the $g-$band bolometric corrections from the evolution of the $g - r$ colors. The resulting light curve peaks at $\simeq 1.24 \times 10^{43}\,\mathrm{erg\,s^{-1}}$, with a maximum occurring at $t^{bol}_{peak} \simeq +9.7$ d, corresponding to a total radiated energy of $\simeq 2.1 \times 10^{49}$ erg within the first 34 d.

An alternative estimate of the luminosity can be obtained using the information on the SED available through the analysis of the spectra at $t \geq +24$ d. We therefore computed $BVRI$ and gri synthetic photometry using the CALCPHOT task available through the IRAF/STSDAS Synthetic Photometry (SYNPHOT) package and fitted black body (BB) functions to the resulting SEDs. Final luminosities were then obtained integrating the fluxes in each band excluding the spectral region at wavelengths shorter than 2000 Å, where the flux is expected to be suppressed by line blanketing (see, e.g., Nicholl et al. 2017). Assuming a power-law decline after $t \simeq 20$ d (see Fig. 1; right panel), we estimated an offset of $2.85 \times 10^{42}\,\mathrm{erg\,s^{-1}}$ between the two methods. Applying this offset to the early light curve would give a peak luminosity of $\simeq 1.5 \times 10^{43}\,\mathrm{erg\,s^{-1}}$ with a total radiated energy of $\simeq 2.8 \times 10^{49}$ erg within the first 34 d and $\simeq 1.4 \times 10^{50}$ erg during the 410 d covered by our follow-up campaign.

Based on the comparison of the +24 d spectrum with the SN templates included in the SuperNova IDentification tool (SNID[9]; Blondin & Tonry 2007, see Sect. 3.2), we compared the main observables of SN 2018ijp at $t \lesssim 20$ d with quantities inferred from samples of SNe Ic-BL, including a simple modeling of the early light curve (see below). Following Lyman et al. (2016, their Eq. 4), the average peak luminosity obtained with the methods described above already suggests a relatively high mass of ^{56}Ni expelled by the SN explosion ($M_{\mathrm{Ni}} \simeq 0.57\,\mathrm{M}_\odot$), although comparable to the average value found by Drout et al. (2011) for their sample of SNe Ic-BL.

The total mass and the kinetic energy of the ejecta can be derived following the prescriptions of Arnett (1982) (see also the formulation of Wheeler et al. 2015 of the analytical model applied to a sample of SE SNe). The model assumes spherical symmetry, a constant optical opacity κ_{opt}, small initial radius ($R_0 \sim 0$) and homologous expansion of the optically thick ejecta $R(t) = R_0 + v_{sc}t$, with v_{sc} being the scale expansion velocity (see Arnett 1982). Under these assumptions, the characteristic time scale $\tau_m = \sqrt{2\tau_0\tau_h}$ can be defined, with τ_0 and τ_h being the diffusion and hydrodynamical times, respectively (see Wheeler et al. 2015). The evolution of the bolometric luminosity can be expressed as a function of the kinetic energy of the ejecta E_k, the ^{56}Ni mass $M_{^{56}\mathrm{Ni}}$ and the total mass of the ejecta M_{ej} as follows (see also Chatzopoulos et al. 2012, and references therein):

$$L_{ph}(t) = M_{^{56}\mathrm{Ni}}\, e^{-x^2} \left[2\,(\epsilon_{^{56}\mathrm{Ni}} - \epsilon_{^{56}\mathrm{Co}}) \int_0^x \xi e^{-\xi \frac{\tau_m}{\tau_{Ni}} + \xi^2} d\xi + \epsilon_{\mathrm{Co}} \int_0^x \xi e^{-\frac{\xi\tau_m}{\tau_{Ni}}\left(1 - \frac{\tau_{Co} - \tau_{Ni}}{\tau_{Co}\tau_{Ni}}\right) + \xi^2} d\xi \right], \quad (1)$$

where $x \equiv t/\tau_m$, $\epsilon_{Co} = 6.78 \times 10^9\,\mathrm{erg\,s^{-1}\,g^{-1}}$ and $\epsilon_{Ni} = 3.90 \times 10^{10}\,\mathrm{erg\,s^{-1}\,g^{-1}}$ (see, e.g., Cappellaro et al. 1997) and τ_{Co}, τ_{Ni} are the radioactive decay times of ^{56}Co and ^{56}Ni (111.3 and 8.8 d, respectively; see, e.g., Nadyozhin 1994). Assuming a constant optical opacity $\kappa_{opt} = 0.07\,\mathrm{cm^2\,g^{-1}}$ (Chugai 2000) and fitting Eq. 1 to the bolometric light curve of SN 2018ijp gives $M_{^{56}Ni} = 0.33 \pm 0.05\,\mathrm{M}_\odot$ and $\tau_m = 4.89 \pm 0.80$ d, which, assuming a constant density within the ejecta, can also be expressed as

[8] http://svo2.cab.inta-csic.es/svo/theory/fps3/

[9] https://people.lam.fr/blondin.stephane/software/snid/

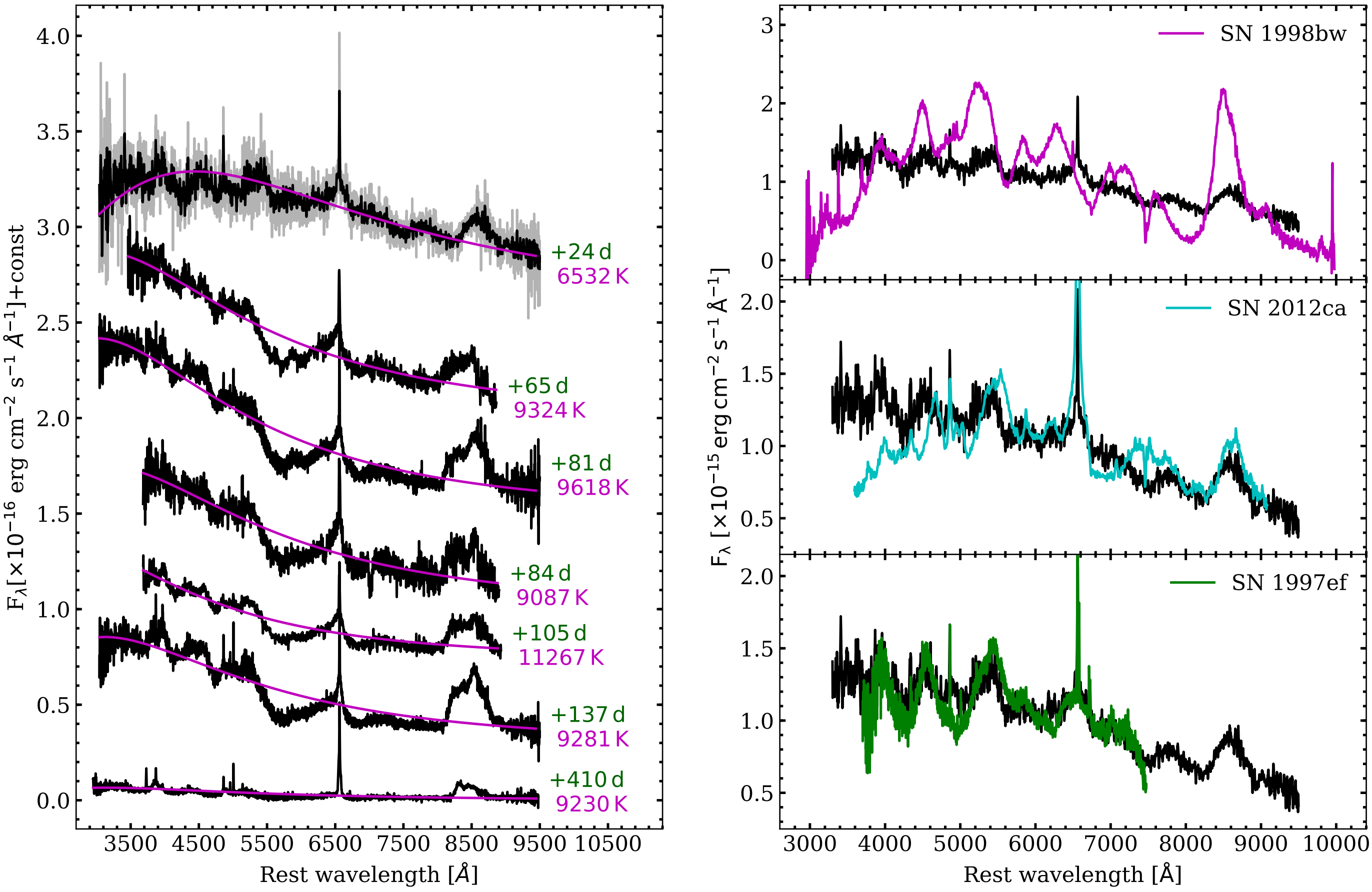

Fig. 2. Left: Low resolution spectra of SN 2018ijp. Rest frame phases refer to the estimated epoch of the explosion. Temperatures were estimated through a BB fit to the spectral continuum. **Right:** Comparison with the +24 d spectrum of SN 2018ijp with those of SNe 1998bw (**top**), 2012ca (**middle**) and 1997ef (**bottom**) at similar phases. The choice of the comparison objects is based on the results obtained with the SNID tool.

follows:

$$\tau_m = \left(\frac{\kappa_{opt}}{\beta c}\right)^{1/2} \left(\frac{3\,M_{ej}^3}{10\,E_k}\right)^{1/4}, \quad (2)$$

where β is an integration constant ($\beta \simeq 13.8$, as in Wheeler et al. 2015). The degeneracy between the kinetic energy and the total mass of the ejecta $E_k = 1/2 M_{ej} < v^2 >$, with $< v^2 >$ being the mean squared expansion velocity, can be broken assuming a constant density within the expanding ejecta and hence $< v^2 >= 3/5 v_{ph}^2$, where v_{ph} is the photospheric velocity as inferred from SN spectral features. An estimate of v_{ph} can be obtained measuring the minima of the P Cygni absorption profiles of Fe II or O I lines (see, e.g. Dessart et al. 2016), which, in the case of SN 2018ijp, corresponds to $v_{\rm O\,I} \simeq 12400\,{\rm km\,s^{-1}}$ (see Sect. 3.2). Following Dessart et al. (2016), this corresponds to $v_{ph} \simeq 21240\,{\rm km\,s^{-1}}$. Taking this value for the photospheric velocity, Eq. 2 then gives $M_{ej} = 1.45 \pm 0.05\,{\rm M_\odot}$ and $E_k = (6.53 \pm 0.35) \times 10^{51}$ erg for the total mass and the kinetic energy of the ejecta.

Although this result might be affected by a non-negligible contribution of ejecta-CSM interaction to the total luminosity, the derived values are consistent with those found by Taddia et al. (2019) for their sample of SNe Ic-BL, with a M_{Ni} and E_k similar to those derived for iPTF15dqg using a similar approach.

At $t > +24$ d, slightly before the onset of the second peak observed in the $g-$ and $r-$ band light curves, the bolometric light curve is well reproduced by a 'broken power-law' starting from +24 d (Fig. 1, right panel), with a break occurring at $\simeq +120$ d. A similar behavior is observed in strongly interacting transients, where the SN shock is expected to break through a dense and extended pre-existing CSM (see, e.g., Fransson et al. 2014; Ofek et al. 2014; Tartaglia et al. 2020, and references therein). The total radiated energy up to +410 d, as well as the prominent narrow Hα line visible at all phases and the high temperatures estimated from the pseudo-continuum of the spectra (Sect. 3.2), also support a CSM interaction interpretation for the second peak of SN 2018ijp. Following Chevalier (1982) and assuming a wind density profile for the CSM ($\rho \propto r^{-2}$), we can therefore estimate the total mass of the CSM surrounding the progenitor star as well as its pre-SN mass-loss rate. Taking $L(t \leq t_{break}) = 3.83 \times 10^{45}\,t^{-0.42}\,{\rm erg\,s^{-1}}$ and assuming $t_{bol}^{peak} = 9.7$ d (the maximum of the estimated bolometric light curve) as the time of the SN shock breakout through the wind, we infer a pre-SN mass-loss rate of $\dot{M} = 0.2\,{\rm M_\odot\,yr^{-1}}$ with a total mass of the swept-up CSM of $0.5\,{\rm M_\odot}$.

The main effect of strong interaction on the observed luminosity is a light curve being dominated by photon diffusion rather than shock-cooling (during the very early phases) or radioactive decays, with the SN shock breaking through the dense CSM rather than the stellar envelope (see, e.g., Balberg & Loeb 2011; Svirski et al. 2012). In the case of SN 2018ijp, at least a fraction of the luminosity output during the first peak could be powered by interaction of the SN ejecta with a moderately massive

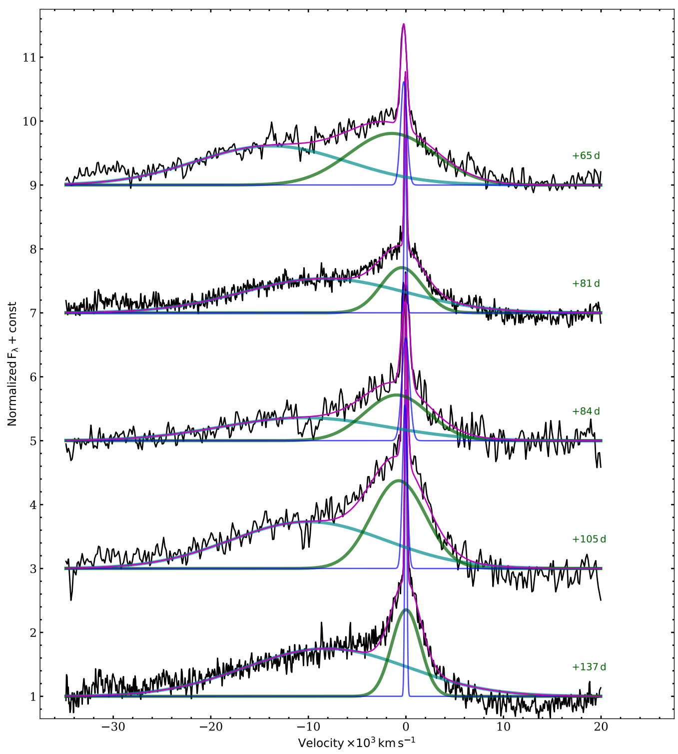

Fig. 3. Evolution of the Hα profile at $t \geq +65$ d, along with a multi-component fit.

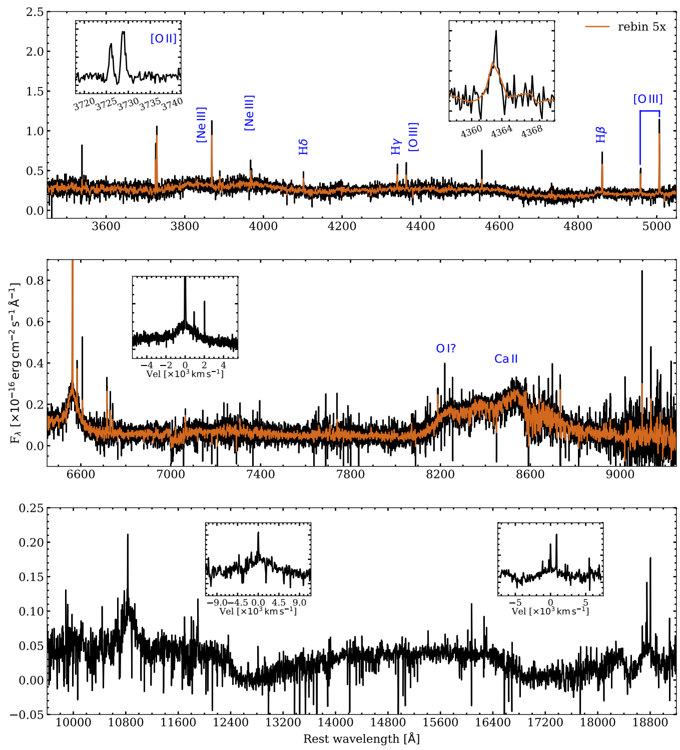

Fig. 4. X-shooter spectra of SN 2018ijp obtained at +178 d. Insets show the [O II] $\lambda\lambda$3727, 3729 and [O III] λ4363 (**upper panel**) and Hα (**middle panel**), He I λ10830 and Paα (**bottom panel**) in velocity space. The NIR spectrum has been re-rebinned to a fifth of its resolution to facilitate the identification of the main emission features.

CSM ($M_{CSM} = 0.5\,M_\odot$, as estimated from the broken power-law fit showed in Fig. 1), with the breakout through the dense wind occurring soon after explosion. On the other hand, this scenario would suggest two distinct stages in the evolution of SN 2018ijp, a first one powered solely by radioactive decay and a second completely dominated by CSM interaction. Although the modeling of the first peak under this assumption (based on the spectral Ic-BL similarity at these phases) gives reasonable results (compared to those obtained by Taddia et al. 2019, for their sample of SNe Ic-BL), we cannot rule out a contribution of the interaction to the total luminosity at $t \lesssim 20$ d. A more complex modeling, beyond the scope of this paper, is probably required to properly model the evolution of SN 2018ijp in order to estimate its explosion parameters.

3.2. Spectroscopy

3.3. Low resolution spectroscopy

Low resolution spectra are shown in Fig. 2 (left panel), along with a tentative fit to the spectral continuum using BBs. This fit is not necessarily indicative of the real temperature of the pseudo-continuum, but is shown to illustrate the evolution of the spectral continuum from +24 d to $t \geq +65$ d.

At +24 d the spectrum is relatively red ($T \simeq 6500$ K) and shows un-resolved Balmer lines in emission (Hα and Hβ) on top of broader features. A tentative line identification performed on the +24 d spectrum reveals the presence of several Fe II multiplets as well as neutral H (Hα to Hδ) and He (λ5875, 6678 and 7065) lines. The lack of other un-resolved features typically associated with H II regions (e.g., [O III], [O II] and [N II]) would suggest that these are recombination lines arising from an un-shocked CSM, although in Sect. 3.4 we show that we cannot rule out a significant contribution from an underlying H II region. Blends of Fe II lines are likely responsible for the "bumps" observed between 4000 and 5000 Å (multiplets 26, 27, 28, 37 and 38) and at $\lambda \sim 5300$ Å (multiplets 42, 48 and 49). Fe II λ5169, typically considered a good proxy of the photospheric velocity of the ejecta (see Dessart & Hillier 2005), shows a narrow, unresolved emission profile, not show the P Cygni profile usually observed in the spectra of other CC SNe, implying a circumstellar origin. Broader absorption features, most likely Fe II, appear blended, forming a typical "w" feature (Liu et al. 2016), making a direct estimate of the ejecta photospheric velocity (through the 5169 Å line) difficult. At $\lambda \gtrsim 7000$ Å the spectrum shows broader features corresponding to O I 7772 − 7775 Å and the NIR Ca II triplet. The minimum of the O I P Cygni absorption corresponds to an expansion velocity of $\simeq 12400$ km s^{-1}, with a blue wing extending up to $\simeq 2 \times 10^4$ km s^{-1}. Following the discussion in Dessart et al. (2016), this corresponds to a photospheric expansion of $\simeq 21240$ km s^{-1}. Figure 2 (right panel) shows a comparison of the +24 d spectrum with those of other SE SNe. A particularly good match, based on the best fit to the spectral features obtained with SNID after "clipping" Hα, was obtained with the Type Ic-BL SN 1997ef (Nomoto et al. 1999; Iwamoto et al. 2000; Mazzali et al. 2000), while the comparison with the Ia-CSM SN 2012ca (Fox et al. 2015; Inserra et al. 2016; Bochenek et al. 2018) does not give such a good match at $\lambda \lesssim 5500$ Å .

At $t \geq 65$ d the spectra show a significant evolution, with the continuum becoming progressively bluer ($T \gtrsim 9000$ K) up to +410 d. We also note a marginal increase in the BB temperature derived at +81 d with respect to the previous epoch

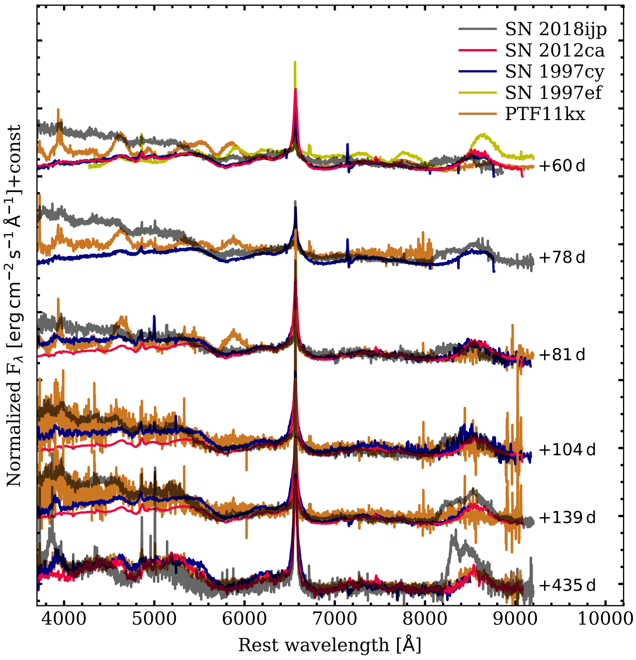

Fig. 5. Comparison of the $t \geq +60$ d (with respect to maximum light) spectral evolution of SN 2018ijp with spectra of SNe 2012ca, 1997cy and PTF11kx obtained at similar phases.

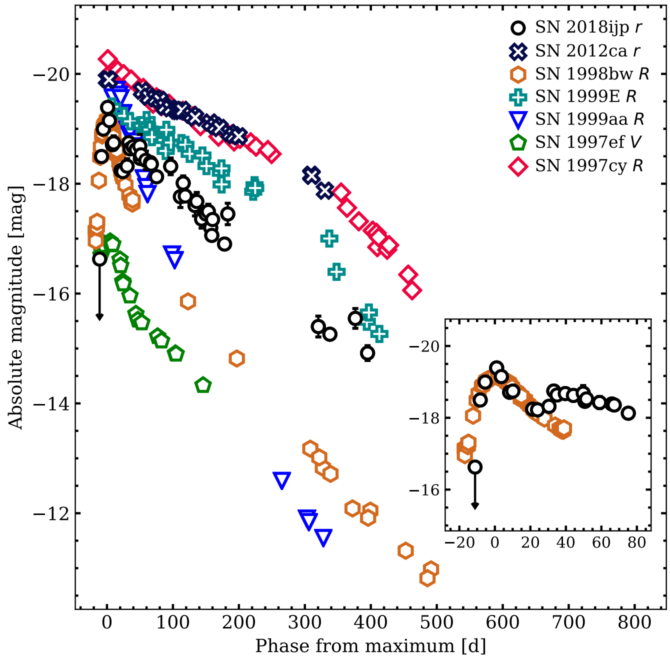

Fig. 6. Comparison of the absolute $r-$band light curve of SN 2018ijp with those of SNe showing similar spectroscopic features. The choice of the reported bands is given in the legend and was made based on the available photometric data for each object. In the inset, a comparison of the early $r-$band light curve of SN 2018ijp with that of SN 1998bw obtained in R.

($\Delta T \simeq 400$ K), although at these phases spectra are dominated by emission lines and hence their pseudo-continuum cannot be reproduced by a BB. While blue excesses can be generally associated to the contribution of fluorescence from numerous blended Fe lines (see, e.g., Tartaglia et al. 2020, and references therein), an increase in the temperature of the pseudo-continuum can also be interpreted as a result of ongoing ejecta-CSM interaction. This interpretation would also be supported by the shape of the bolometric light curve (Fig. 1, right panel), showing a “broken power-law" shape typical of interacting SNe.

The total luminosity of Hα (measured in the 6000 − 7000 Å range) at +65 d ($\simeq$ 1.1×10^{41} erg s^{-1}) also shows a drastic increase with respect to the previous epoch ($L_{H\alpha,+24\,\mathrm{d}} \simeq 2.8 \times 10^{40}$ erg s^{-1}), subsequently remaining roughly constant up to +137 d. In the last spectrum, on the other hand, we note a decrease, with the luminosity returning roughly to the same value as observed at +24 d ($\simeq 3 \times 10^{40}$ erg s^{-1}). This, along with the simultaneous presence of other prominent host lines (e.g., [O iii] and [O ii]) at +410 d, may also suggest that narrow H features observed at +24 d were due to host contamination and the lack of other galactic lines at +24 d was mostly due to the low S/N of the spectrum.

A “delayed interaction" might be explained by the presence of a confined dense shell surrounding the progenitor star of SN 2018ijp. Assuming that the onset of strong ejecta-CSM interaction is at $t \simeq +25$ d (according to the evolution of the bolometric light curve and immediately after the epoch of the first spectrum), and a constant expansion velocity of $v = v_{ph} \simeq 21240$ km s^{-1} (see above), the shell would be located at a distance of $\simeq 4.6 \times 10^{15}$ cm from the progenitor star of SN 2018ijp. This estimate is at the same order of magnitude as that inferred from the BB fit performed at +65 d ($\simeq 10^{15}$ cm). Under the same assumptions, we could argue that the SN shock breaks through the confined shell roughly at $t \simeq 273.5$ d, implying an external radius of the shell of $\simeq 5 \times 10^{16}$ cm. This detached H-rich shell might be produced by a single massive progenitor during its red supergiant phase and hence expelled 10 − 100 yr before CC (see, e.g., Margutti et al. 2017, for a similar interpretation for SN 2014C), or the last eruptive episode of a Wolf-Rayet star in its transitional phase from the LBV phase (see, e.g., the case of the Type Ibn SN 2006jc; Pastorello et al. 2007). On the other hand, we cannot rule out that such medium was originated by binary interactions or through the ejection of a fraction of the mass of the system during a common-envelope phase.

In Fig. 3 we show the evolution of the spectral region around Hα at +65 d $\leq$ t $\leq$ +137 d, revealing a structured and asymmetric profile throughout the spectroscopic evolution of the transient. A multi-gaussian fit reveals two broad components: a blue-shifted component with a FWHM of $\simeq 2 \times 10^4$ km s^{-1} and a redder one with a FWHM slowly decreasing from $\simeq 10^4$ to $\simeq 3 \times 10^3$ km s^{-1}, with a third narrow and unresolved component. While the redder component is likely due to the wings of the typical electron scattering profile observed in high-resolution spectra of interacting transients (see, e.g., Huang & Chevalier 2018), its velocity is consistent with those typically observed in shocked regions of dense media typically surrounding the progenitors of SNe IIn. A clumpy (e.g., Chugai & Danziger 1994) or highly asymmetric (e.g., Smith et al. 2014) CSM, would explain the simultaneous presence of a broad component, which would then be produced by the outer ionized layers of the freely expanding SN ejecta and an intermediate component arising from the shocked CSM, with the narrow emission feature possibly produced in the ionized un-shocked wind (see, e.g. Turatto et al. 1993, although see Sect. 3.4 for an alternative explanation for the narrow Hα component).

Table 1. Log of the spectroscopic observations of SN 2018ijp

Date	JD	Phase (d)	Instrumental setup	Grism/Grating	Spectral range (Å)	Resolution ($\lambda/\Delta\lambda$)	Exposure time (s)
20181201	2458454.08	+24 d	Keck1+LRIS	400/3400+400/8500	3500 – 10000	900	300 + 300
20190115	2458498.64	+65 d	NOT+ALFOSC	Gr4	4000 – 10000	300	2700
20190201	2458516.03	+81 d	Keck1+LRIS	400/3400+400/8500	3500 – 10000	860	600 + 600
20190204	2458519.58	+84 d	NOT+ALFOSC	Gr4	4000 – 10000	320	2700
20190227	2458542.44	+105 d	NOT+ALFOSC	Gr4	4000 – 10000	400	2 × 2700
20190503	2458606.91	+178 d	VLT+Xshooter	UVB+VIS+NIR	3500 – 20000	5400 + 8900 + 5600	3 × (1200 + 1262 + 300)
20190403	2458576.89	+137 d	Keck1+LRIS	400/3400+400/8500	3500 – 10000	800	300 + 300
20200124	2458873.02	+410 d	Keck1+LRIS	400/3400 + 400/8500	3500 – 10000	850	1375

Notes. NOT: 2.56 m Nordic Optical Telescope with ALFOSC; VLT: 8 m Very Large Telescope with X-shooter (ESO Observatorio del Paranal, Chile); KECK: 10 m Keck I telescope with LRIS (Mauna Kea Observatory, Hawaii - U.S.A.). . Data will be released through the Weizmann Interactive Supernova data REPository (WISEREP[a]; Yaron & Gal-Yam 2012)

[a] https://wiserep.weizmann.ac.il/

3.4. The X-shooter spectrum

Medium resolution spectra were obtained with X-shooter around 2019 May 3.41 UT (JD = 2458606.91, t = +178 d). The observations consist of three combined spectra obtained with the UVB, VIS and NIR arms covering 300 – 560, 560 – 1024 and 1024 – 2480 nm, respectively[10], with each spectrum obtained by median combining three different exposures. Each observation was obtained at airmass $\lesssim 1.5$, at an average seeing of 0.″7 and we therefore take the nominal values of resolution of each spectrum (R $\equiv \lambda/\Delta\lambda$ = 5400, 8900 and 5600 in the UVB, VIS and NIR arm, respectively, for slit widths of 1.″0 in UVB and 0.″9 in VIS and NIR)[11]. The resulting spectra are shown in Fig. 4.

The Hα region shows a structured profile with a narrow (FWHM $\simeq$ 70 km s^{-1}) component on top of a broader (FWHM $\simeq$ 1240 km s^{-1}) and slightly blue-shifted ($v_{shift} \simeq$ 300 km s^{-1}) one. The measured Hα/Hβ line ratio is 2.8, consistent with the predicted Balmer decrement in a Case B recombination scenario (assuming T = 10^4 K and n_e = 10^2 cm^{-3}; see Osterbrock & Ferland 2006), confirming the negligible contribution of the local environment to the total extinction in the direction of SN 2018ijp.

A much shallower broad component is observed in Hβ, where a tentative fit revealed a broader component with a higher FWHM of $\simeq$ 2130 km s^{-1} and a marginally resolved narrow component with a FWHM $\simeq$ 70 km s^{-1}. The FWHM derived from the narrow Hα and Hβ components are comparable to those inferred from the FWHM of all the other host lines (e.g. [O II] $\lambda\lambda$3726, 3729, [O III] λ4363, 4958 and 5007, [Ne III] λ3868 and 3967), suggesting that these are possibly emitted in an underlying H II region. This, in turn, seems to suggest that the narrow Hα components observed throughout the spectroscopic evolution of SN 2018ijp are all affected by host galaxy contamination. Assuming that the entire narrow Hα component is due to the contamination of the local environment of SN 2018ijp, its flux can be used to infer an estimate of the local star-formation rate (SFR), using the relation SFR(M$_\odot$ yr^{-1}) = $7.9 \times 10^{-42} L_{H\alpha}\left[\mathrm{erg\,s^{-1}}\right]$ (see, e.g., Kennicutt 1998), resulting in SFR$_{\rm local}$ = 2.7×10^{-2} M$_\odot$ yr^{-1}. Using the N2 emission line diagnostic (Pettini & Pagel 2004) and following the prescriptions of Marino et al. (2013), we also estimate a local sub-solar metallicity of 12 + log(O/H) = 8.42 ± 0.04 dex (taking 12 + log(O/H)$_\odot$ = 8.69 dex; see Asplund et al. 2009), similar to the values obtained by Modjaz et al. (2020) for their PTF sample of SNe Ic-BL.

The [O III] λ4363 line is clearly detected, although this line is usually faint compared to [O III] $\lambda\lambda$4959, 5007, with $(j_{5007} + j_{4959})/j_{4363} \gtrsim 50$ in typical H II regions and can be >> 50 in galaxies hosting CC interacting SNe (see, e.g., Fransson et al. 2014, and references therein). The inferred value for SN 2018ijp is $(j_{5007}+j_{4959})/j_{4363} = 7.2$, implying very high temperatures and densities for the emitting gas (e.g., $T_e \gtrsim 2.7\times10^4$ K for electron densities $n_e \gtrsim 10^6$ cm^{-3} in a 5-level atom approximation; see De Robertis et al. 1987; Shaw & Dufour 1995). This seems to suggest a circumstellar origin for the [O III] lines. The measured [O II] line ratio (j_{3729}/j_{3726} = 1.26), corresponds to an electron density $n_e \simeq 10^2$ cm^{-3} (see Osterbrock & Ferland 2006), revealing a non-negligible contribution of the local environment to the flux of the forbidden O lines, with the measured [O III] flux probably arising from both regions and implying an even lower $(j_{5007} + j_{4959})/j_{4363}$ ratio.

3.5. On the nature of SN 2018ijp

In the previous Sections we presented the peculiar photometric and spectroscopic evolution of SN 2018ijp and discussed its observables, favoring a scenario of a Type Ic-BL SN exploding within a dense pre-existing CSM. Despite strong signatures of interaction at $t \geq$ +65 d, the analysis of the spectrum at +24 d provides a very good match with the Type Ic-BL SN 1997ef (see Fig. 2). This gives clues about the nature of the explosion mechanism triggering SN 2018ijp, suggesting the CC of a stripped massive star as a viable progenitor for SN 2018ijp.

At later times, the spectral evolution of SN 2018ijp closely resemble those of SN 1997cy (Turatto et al. 2000; Germany et al. 2000) and other similar transients, while the match is not as good for the Ia-CSM SN PTF11kx (Dilday et al. 2012) at +60 d $\leq$ t $\leq$ +81 d (with respect to maximum light), or for the Type Ic SN 1997ef itself (see Fig. 5), suggesting a spectral shape completely dominated by ongoing SN ejecta-CSM interaction (i.e., a blue continuum with prominent narrow recombination lines). The analysis of the spectral region around the Hα line (Fig. 3), suggests the presence of a very broad, blue-shifted component, marginally visible since +24 d (see Fig. 2). This is at odds with a Type Ic origin if interpreted as fast-moving H-rich SN ejecta, with a significantly higher value (more than a factor of 2) with respect to those typically inferred from Hα in Type II

[10] https://www.eso.org/sci/facilities/paranal/instruments/xshooter/overview.html
[11] https://www.eso.org/sci/facilities/paranal/instruments/xshooter/inst.html

SNe (see, e.g., the median value for the sample of Type II SNe of Gutiérrez et al. 2017).

On the other hand, a high optical depth by incoherent electron scattering in the post-shock region could be able to explain the extended blue wing in Hα without invoking alternative interpretations for the observables of SN 2018ijp. A combined effect of a high optical depth and the shock velocity was also discussed by Taddia et al. (2020, see their Fig. 22) in order to explain the similarly structured Hα profile of SN 2013L. In this scenario, while the slope of the blue wing is strongly affected by the optical depth of the CSM, the suppression of the flux at redder wavelengths is caused by the efficient thermalization (obscuration) of the Hα photons in the SN ejecta.

Where the early spectral comparison seems to suggest the collapse of a stripped massive star as the most plausible progenitor of SN 2018ijp, a comparison of the absolute luminosities is also consistent with such a scenario (Fig. 6). At $t \lesssim 30$ d, in particular, the photometric evolution of SN 2018ijp resembles that of the Ic-BL SN 1998bw, although with an apparent faster rise to maximum, supporting a Ic-CSM scenario with the late-time light curve dominated by the progressively stronger effects of ejecta-CSM interaction. Interaction as the dominant source of luminosity would explain the dramatic evolution in the observed spectral continuum from +24 and +65 d (see Sect. 3.2 and Fig. 2), as well as the shape of the bolometric light curve at $t \gtrsim 25$ d (see Fig. 1, right panel). In this context, the photometric evolution of SN 2018ijp can be divided in two main phases, a first one dominated by radioactive decays, suggesting a mass of expelled radioactive ^{56}Ni of 0.3 $M_\odot$ with respect to a total ejected mass of 1.5 $M_\odot$ and kinetic energy of 6.5×10^{51}, erg and an interaction-dominated phase where the SN ejecta collide with a 0.5 $M_\odot$ H-rich pre-existing CSM (see Sect. 3.1.1). The early features observed in SN 2018ijp, with high expansion velocities measured from the +24 d spectrum, as well as the relatively high masses of radioactive ^{56}Ni and pre-existing CSM, seem to support a massive star, most likely a WR, as its progenitor, with the CSM either produced during a previous evolutionary stage or by binary interactions with a lower-mass, H-rich companion.

Acknowledgements. Based on observations obtained with the Samuel Oschin Telescope 48-inch and the 60-inch Telescope at the Palomar Observatory as part of the Zwicky Transient Facility project. Major funding has been provided by the U.S National Science Foundation under Grant No. AST-1440341 and by the ZTF partner institutions: the California Institute of Technology, the Oskar Klein Centre, the Weizmann Institute of Science, the University of Maryland, the University of Washington, Deutsches Elektronen-Synchrotron, the University of Wisconsin-Milwaukee, and the TANGO Program of the University System of Taiwan. The data presented here were partly obtained with ALFOSC, which is provided by the Instituto de Astrofisica de Andalucia (IAA) under a joint agreement with the University of Copenhagen and NOTSA.
The Liverpool Telescope is operated on the island of La Palma by Liverpool John Moores University in the Spanish Observatorio del Roque de los Muchachos of the Instituto de Astrofisica de Canarias with financial support from the UK Science and Technology Facilities Council.
This research has made use of the NASA/IPAC Extragalactic Database (NED), which is funded by the National Aeronautics and Space Administration and operated by the California Institute of Technology.
This research has made use of the NASA/IPAC Infrared Science Archive, which is funded by the National Aeronautics and Space Administration and operated by the California Institute of Technology.
This research has made use of the SVO Filter Profile Service (http://svo2.cab.inta-csic.es/theory/fps/) supported from the Spanish MINECO through grant AYA2017-84089
IRAF is distributed by the National Optical Astronomy Observatory, which is operated by the Association of Universities for Research in Astronomy (AURA) under a cooperative agreement with the National Science Foundation.
SNOoPy is a package for SN photometry using PSF fitting and/or template subtraction developed by E. Cappellaro. A package description can be found at http://sngroup.oapd.inaf.it/snoopy.html.
FOSCGUI is a graphic user interface aimed at extracting SN spectroscopy and photometry obtained with FOSC-like instruments. It was developed by E. Cappellaro. A package description can be found at http://sngroup.oapd.inaf.it/foscgui.html.

References

Arnett, W. D. 1982, ApJ, 253, 785
Asplund, M., Grevesse, N., Sauval, A. J., & Scott, P. 2009, ARA&A, 47, 481
Balberg, S. & Loeb, A. 2011, MNRAS, 414, 1715
Bellm, E. C., Kulkarni, S. R., Graham, M. J., et al. 2019, PASP, 131, 018002
Benetti, S., Cappellaro, E., Turatto, M., et al. 2006, ApJ, 653, L129
Blondin, S. & Tonry, J. L. 2007, ApJ, 666, 1024
Bochenek, C. D., Dwarkadas, V. V., Silverman, J. M., et al. 2018, MNRAS, 473, 336
Cappellaro, E., Mazzali, P. A., Benetti, S., et al. 1997, A&A, 328, 203
Cardelli, J. A., Clayton, G. C., & Mathis, J. S. 1989, ApJ, 345, 245
Chatzopoulos, E., Wheeler, J. C., & Vinko, J. 2012, ApJ, 746, 121
Chen, T. W., Inserra, C., Fraser, M., et al. 2018, ApJ, 867, L31
Chevalier, R. A. 1982, ApJ, 258, 790
Chugai, N. N. 2000, Astronomy Letters, 26, 797
Chugai, N. N. & Danziger, I. J. 1994, MNRAS, 268, 173
De Robertis, M. M., Dufour, R. J., & Hunt, R. W. 1987, JRASC, 81, 195
Dekany, R., Smith, R. M., Riddle, R., et al. 2020, PASP, 132, 038001
Dessart, L. & Hillier, D. J. 2005, A&A, 439, 671
Dessart, L., Hillier, D. J., Woosley, S., et al. 2016, MNRAS, 458, 1618
Dilday, B., Howell, D. A., Cenko, S. B., et al. 2012, Science, 337, 942
Drout, M. R., Soderberg, A. M., Gal-Yam, A., et al. 2011, ApJ, 741, 97
Fox, O. D., Silverman, J. M., Filippenko, A. V., et al. 2015, MNRAS, 447, 772
Fransson, C., Ergon, M., Challis, P. J., et al. 2014, ApJ, 797, 118
Fremling, C., Sollerman, J., Taddia, F., et al. 2016, A&A, 593, A68
Freudling, W., Romaniello, M., Bramich, D. M., et al. 2013, A&A, 559, A96
Germany, L. M., Reiss, D. J., Sadler, E. M., Schmidt, B. P., & Stubbs, C. W. 2000, ApJ, 533, 320
Graham, M. J., Kulkarni, S. R., Bellm, E. C., et al. 2019, PASP, 131, 078001
Gutiérrez, C. P., Anderson, J. P., Hamuy, M., et al. 2017, ApJ, 850, 89
Hamuy, M., Phillips, M. M., Suntzeff, N. B., et al. 2003, Nature, 424, 651
Heger, A., Fryer, C. L., Woosley, S. E., Langer, N., & Hartmann, D. H. 2003, ApJ, 591, 288
Hogg, D. W., Baldry, I. K., Blanton, M. R., & Eisenstein, D. J. 2002, arXiv e-prints, astro
Hosseinzadeh, G., McCully, C., Zabludoff, A. I., et al. 2019, ApJ, 871, L9
Huang, C. & Chevalier, R. A. 2018, MNRAS, 475, 1261
Inserra, C., Fraser, M., Smartt, S. J., et al. 2016, MNRAS, 459, 2721
Iwamoto, K., Nakamura, T., Nomoto, K., et al. 2000, ApJ, 534, 660
Kennicutt, Robert C., J. 1998, ARA&A, 36, 189
Kuncarayakti, H., Maeda, K., Ashall, C. J., et al. 2018, ApJ, 854, L14
Liu, Y.-Q., Modjaz, M., Bianco, F. B., & Graur, O. 2016, ApJ, 827, 90
Lyman, J. D., Bersier, D., & James, P. A. 2014, MNRAS, 437, 3848
Lyman, J. D., Bersier, D., James, P. A., et al. 2016, MNRAS, 457, 328
Margutti, R., Kamble, A., Milisavljevic, D., et al. 2017, ApJ, 835, 140
Marino, R. A., Rosales-Ortega, F. F., Sánchez, S. F., et al. 2013, A&A, 559, A114
Mazzali, P. A., Iwamoto, K., & Nomoto, K. 2000, ApJ, 545, 407
Milisavljevic, D., Margutti, R., Kamble, A., et al. 2015, ApJ, 815, 120
Modjaz, M., Bianco, F. B., Siwek, M., et al. 2020, ApJ, 892, 153
Modjaz, M., Blondin, S., Kirshner, R. P., et al. 2014, AJ, 147, 99
Nadyozhin, D. K. 1994, ApJS, 92, 527
Nicholl, M., Guillochon, J., & Berger, E. 2017, ApJ, 850, 55
Nomoto, K., Iwamoto, K., Mazzali, P. A., & Nakamura, T. 1999, Astronomische Nachrichten, 320, 265
Ofek, E. O., Zoglauer, A., Boggs, S. E., et al. 2014, ApJ, 781, 42
Oke, J. B., Cohen, J. G., Carr, M., et al. 1994, Low-Resolution Imaging Spectrometer for the Keck Telescope, Vol. 2198 (Society of Photo-Optical Instrumentation Engineers (SPIE) Conference Series), 178–184
Osterbrock, D. E. & Ferland, G. J. 2006, Astrophysics of gaseous nebulae and active galactic nuclei (University Science Books, 2006)
Pastorello, A., Smartt, S. J., Mattila, S., et al. 2007, Nature, 447, 829
Pastorello, A., Wang, X. F., Ciabattari, F., et al. 2016, MNRAS, 456, 853
Perley, D. A. 2019, PASP, 131, 084503
Pettini, M. & Pagel, B. E. J. 2004, MNRAS, 348, L59
Rodrigo, C., Solano, E., & Bayo, A. 2012, SVO Filter Profile Service Version 1.0, IVOA Working Draft 15 October 2012
Schlafly, E. F. & Finkbeiner, D. P. 2011, ApJ, 737, 103
Schlegel, E. M. 1990, MNRAS, 244, 269
Shaw, R. A. & Dufour, R. J. 1995, PASP, 107, 896
Silverman, J. M., Nugent, P. E., Gal-Yam, A., et al. 2013, ApJS, 207, 3
Smartt, S. J. 2009, ARA&A, 47, 63
Smith, N., Hinkle, K. H., & Ryde, N. 2009, AJ, 137, 3558
Smith, N., Mauerhan, J. C., & Prieto, J. L. 2014, MNRAS, 438, 1191
Svirski, G., Nakar, E., & Sari, R. 2012, ApJ, 759, 108
Taddia, F., Sollerman, J., Fremling, C., et al. 2019, A&A, 621, A71
Taddia, F., Sollerman, J., Leloudas, G., et al. 2015, A&A, 574, A60
Taddia, F., Stritzinger, M. D., Fransson, C., et al. 2020, arXiv e-prints, arXiv:2003.09709
Tartaglia, L., Pastorello, A., Sollerman, J., et al. 2020, A&A, 635, A39
Turatto, M., Cappellaro, E., Danziger, I. J., et al. 1993, MNRAS, 262, 128
Turatto, M., Suzuki, T., Mazzali, P. A., et al. 2000, ApJ, 534, L57
Vernet, J., Dekker, H., D'Odorico, S., et al. 2011, A&A, 536, A105
Wheeler, J. C., Johnson, V., & Clocchiatti, A. 2015, MNRAS, 450, 1295
Wright, E. L. 2006, PASP, 118, 1711
Yaron, O. & Gal-Yam, A. 2012, PASP, 124, 668
Yoon, S.-C. & Cantiello, M. 2010, ApJ, 717, L62